Nanoscale

PAPER

View Article Online
View Journal | View Issue

Cite this: *Nanoscale*, 2014, **6**, 10798

Nanoporous silicon nitride membranes fabricated from porous nanocrystalline silicon templates

J. P. S. DesOrmeaux,†[a] J. D. Winans,†*[b] S. E. Wayson,[b] T. R. Gaborski,[c] T. S. Khire,[b] C. C. Striemer[a] and J. L. McGrath*[b]

Received 4th June 2014
Accepted 16th July 2014

DOI: 10.1039/c4nr03070b

www.rsc.org/nanoscale

The extraordinary permeability and manufacturability of ultrathin silicon-based membranes are enabling devices with improved performance and smaller sizes in such important areas as molecular filtration and sensing, cell culture, electroosmotic pumping, and hemodialysis. Because of the robust chemical and mechanical properties of silicon nitride (SiN), several laboratories have developed techniques for patterning nanopores in SiN using reactive ion etching (RIE) through a template structure. These methods however, have failed to produce pores small enough for ultrafiltration (<100 nm) in SiN and involve templates that are prone to microporous defects. Here we present a facile, wafer-scale method to produce nanoporous silicon nitride (NPN) membranes using porous nanocrystalline silicon (pnc-Si) as a self-assembling, defect free, RIE masking layer. By modifying the mask layer morphology and the RIE etch conditions, the pore sizes of NPN can be adjusted between 40 nm and 80 nm with porosities reaching 40%. The resulting NPN membranes exhibit higher burst pressures than pnc-Si membranes while having 5× greater permeability. NPN membranes also demonstrate the capacity for high resolution separations (<10 nm) seen previously with pnc-Si membranes. We further demonstrate that human endothelial cells can be grown on NPN membranes, verifying the biocompatibility of NPN and demonstrating the potential of this material for cell culture applications.

Introduction

Nanoporous membranes serve a critical role in a wide range of applications including optical and biological sensing, chemical processing for fuel cells and bioreactors, and separations for desalination, dialysis, protein purification, and controlled drug delivery.[1,2] The majority of separations requiring nanoscale pores are accomplished using polymer ultrafiltration membranes.[3] Ultrafiltration membranes are typically made by solvent casting such that a thin nanoporous skin ~500 nm is supported by a thicker microporous substructure. The resolution of polymer membranes suffers from an intrinsic log-normal pore size distribution.[4] The tortuous path pore structure also adds flow resistance and increases the amount of surface area to which valuable process material can bind.

A number of commercial technologies produce membranes with pore distributions that are more uniform than conventional ultrafiltration membranes. The oldest example dates back to the 1970's and the invention of nuclear track etch (TE) membranes[5] in which a dense polycarbonate membrane is bombarded with high-energy particles and then chemically etched along the resulting defect lines (tracks) to make pores. TE membranes are commercially available in pore sizes appropriate for ultrafiltration (10 nm–100 nm), however with a relatively low pore density of 6×10^8 pores per cm^2 and a thickness of ~5 um, the hydraulic permeability of TE membranes is quite low (~1 mL min^{-1} cm^{-2} bar^{-1} for 30 nm pores). An alternative commercial material electrochemically etches pores into alumina oxide to create membranes with reasonably uniform pores, with average pore sizes of 10–200 nm, and a much higher pore density than track etched membranes (10^{11} pores per cm^2). These membranes must be much thicker (~60 μm) to achieve mechanical robustness (Lee, Ji *et al.* 2006, Osmanbeyoglu, Hur *et al.* 2009) and as a consequence the hydraulic permeability of commercially available filters with 20 nm pores is 5.8 mL min^{-1} cm^{-2} bar^{-1}.[6]

In 2007 we introduced porous nanocrystalline silicon (pnc-Si) as a new type of nanoporous membrane where the pores are formed spontaneously during the crystallization of ultrathin a-Si films.[7] Pnc-Si membranes exhibit extraordinary hydraulic and diffusive permeabilities because of their molecular-scale (~15–30 nm) thinness. Pnc-Si is also capable of high-resolution separations (~5 nm) because the pore distributions display sharp cut-offs.[8,9] The cut-off pore diameter for pnc-Si closely follows the membrane thickness,[8] and the membranes have high pore densities (10^{10} pores per cm^2) and porosities (~15%).

[a]*SiMPore, West Henrietta, NY 14586, USA*

[b]*Department of Biomedical Engineering, University of Rochester, Rochester, NY 14627, USA. E-mail: j.winans@rochester.edu; jmcgrath@bme.rochester.edu*

[c]*Department of Biomedical Engineering, Rochester Institute of Technology, Rochester, NY 14623, USA*

† These authors contributed equally.

In addition to separations, pnc-Si membranes have been used as cell culture substrates,[10] as electroosmotic pumps,[11] as porous electrodes in capacitance-based sensors,[12] and as a nanoporous element for DNA sequencing.[13] The primary limitation of the pnc-Si platform is the mechanical weakness of large membrane areas. While small membranes (<0.04 mm^2) exhibit burst pressures exceeding 1 ATM,[7] larger areas can be too weak for practical use and require additional scaffold support.[14]

Silicon nitride (SiN) is commonly selected for thin film microfabrication because it is more mechanically robust and more chemically inert than alternatives. The mechanical strength of SiN has enabled free-standing thin films including microporous[15] and nanoporous membranes.[16] While micron-sized pores can be patterned using standard photolithography, nanoporous membranes require more innovative techniques. The first nanoporous SiN membranes were produced by direct ablation using a focused ion beam,[16] a process far too time consuming for commercial manufacturing.[7] More recently, Vlassiouk *et al.* used the track etch technique to form SiN membranes with a similar pore morphology, porosity and separation characteristics as pnc-Si.[17] However, because the track-etch process requires access to a special synchrotron using large ions, industrial scale manufacturing presents many challenges.

An emerging approach to wafer scale fabrication of nanoporous SiN membranes involves the use of self-assembling nanoparticles[18,19] as pore templates. In this technique, a wafer is covered in nanoparticles by the agglomeration of a thin metal film or by spin-coating a suspension. This is followed by the deposition of chromium to create a reverse image of the particle field. The patterned chromium layer is then used as a RIE mask for the underlying SiN. The process is highly dependent on a well-controlled nanoparticle preparation; any debris or particle agglomerate will become a hole during mask reversal and a membrane defect after the pore transfer process. To date, the pore size cut-offs created by nanoparticle templating methods have been greater than 100 nm, a size too large for ultrafiltration applications.[20] Nanoimprint lithography has also been used in combination with RIE to create SiN membranes with 400 nm pores.[21] Unlike self-assembled templates, nanoimprinting enables pore position and sizes to be directly patterned. However, the published technique is very complex, requiring several additive, subtractive, and RIE processes to accomplish pore transfer.

In this paper we present a novel wafer-scale process for the fabrication of defect-free NPN membranes. We recently demonstrated that it is possible to form pnc-Si by crystalizing amorphous silicon on a SiN layer[22] instead of the original SiO_2 layer.[7] In this work we take advantage of this structure to create NPN membranes using pnc-Si as a pore template. Our work examines the effects RIE gas composition, pnc-Si formation temperature, and etch times on the transfer of pnc-Si pores to underlying SiN. Samples are also evaluated for burst pressure, gas permeance, hydraulic permeability, and separation of Au NPs. Finally, cells are grown on the membranes prepared with different RIE etch times to examine biocompatibility. The results demonstrate that NPN membranes prepared using a pnc-Si template have slightly larger pores and higher porosity than pnc-Si. NPN membranes share the excellent flow and separation characteristics of pnc-Si while being markedly stronger and more chemically stable.

Results and discussion

Process optimization

Two preliminary steps were necessary before attempting to use pnc-Si as a mask for RIE-based pore transfer to SiN (Fig. 1a). First we formed 40 nm pnc-Si in a traditional SiO_2–Si–SiO_2 stack. Our prior work had demonstrated that through-pores form in 30 nm nanocrystalline silicon but we had not attempted pore formation in thicker films.[8] Maximizing the thickness of the pnc-Si layer enables the longest possible etch through SiN before the loss of the pnc-Si mask. Fig. 1a provides a representative TEM micrograph of the resulting 40 nm pnc-Si. Using custom MATLAB code for pore analysis (http://nanomembranes.org/software/) the average pore size and porosity were calculated to be 40 nm and 6.5%, respectively.

In the next step, the same 40 nm pnc-Si was formed using a membrane stack of SiN–Si–SiO_2 in order to confirm that similar pore formation would take place with the a-Si layer adjacent to SiN instead of SiO_2. Fig. 1b is an SEM micrograph showing the cross-section of a film consisting of 40 nm thick pnc-Si directly on top of a 50 nm thick SiN after the top SiO_2 layer has been chemically removed. The open pores are clearly visible as dark regions in the upper layer of this cross-section.

NPN membranes were fabricated using standard semiconductors processes as illustrated in Fig. 2. A wafer coated on

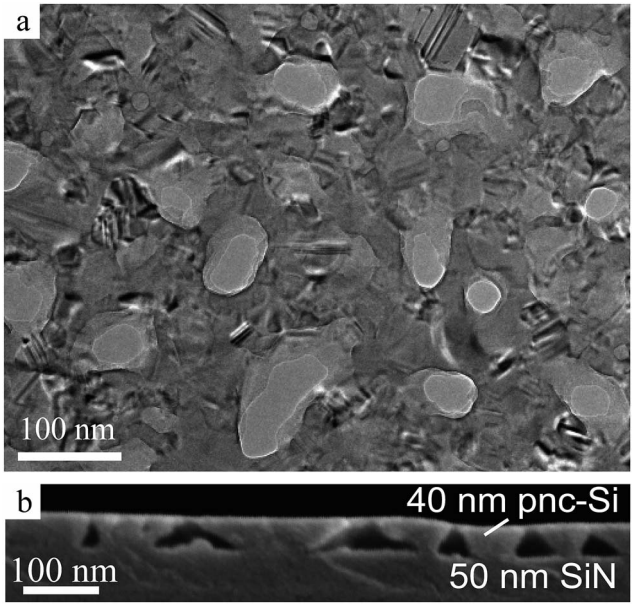

Fig. 1 (a) TEM micrograph of 40 nm pnc-Si formed in a traditional SiO_2–Si–SiO_2 stack. Light gray areas are the open pores and the darker regions are indicative of nanocrystalline Si. (b) SEM micrograph showing the cross-sectional view of 40 nm pnc-Si formed on top of a SiN film.

both sides with 50 nm SiN, received a sputtered film of 40 nm-thick amorphous silicon followed by a 20 nm-thick SiO_2 film, as shown in Fig. 2a. The wafers next underwent a rapid thermal process (RTP), which leads to pnc-Si formation on top of the SiN (Fig. 2b). Fig. 2c illustrates how the backside SiN was patterned using standard photolithography. After patterning the backside, the top layer of SiO_2 was removed. The nanopores present in the pnc-Si film were then transferred into the underlying SiN layer using a RIE process, as seen in Fig. 2d. Next, a 100 nm-thick SiO_2 layer was deposited on top of the nanoporous film *via* PECVD using tetraethyl orthosilicate (TEOS) as a precursor gas. The SiO_2 layer protects the nanoporous film during the bulk Si wafer etch necessary to create the freestanding membranes pictured in Fig. 2e. Finally, the protective SiO_2 is removed and the NPN membranes are ready for use. All membranes used in this work are formed on chips that are 5.4 mm square with 5 separate slots of measuring 0.1 × 3 mm. The total active area of the chip is 1.5 mm^2.

We examined the influence of a range of manufacturing parameters on NPN pore size and pore density. The first parameter examined was the pressure setting in the RIE chamber. The pressure was tested at 100, 200, and 300 mTorr on sections of bulk wafers with 40 nm pnc-Si on 50 nm SiN that were not etched to form freestanding membranes. The SEM micrographs in Fig. 3a–c show an increase in transferred pore size with increasing pressure in both the top down view as well as the cross-sections as the pressure increases from 100, 200 and 300 mTorr, respectively. Because the goal of this work is to transfer pores from pnc-Si to SiN as precisely as possible, we chose to use the less aggressive 100 mTorr for all subsequent tests.

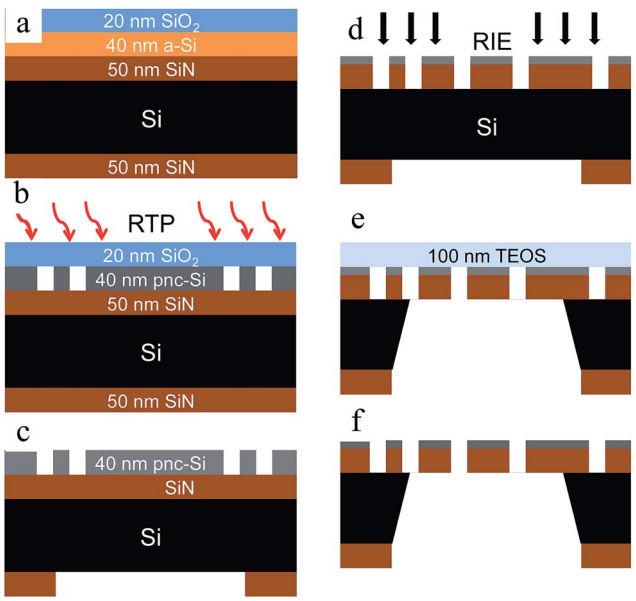

Fig. 2 A diagram of the fabrication process flow. (a) 200 μm wafer with 50 nm LPCVD SiN on both sides and sputtered 40 nm a-Si and 20 nm SiO_2 on the front side. (b) The RTP process forming the pnc-Si. (c) Patterning of the backside and the removal of the front SiO_2 film. (d) RIE pore transfer. (e) A PECVD TEOS oxide film is deposited on the front side followed by an EDP etch of substrate to define the window sizes and the chip dimensions. (f) Schematic of the final chip.

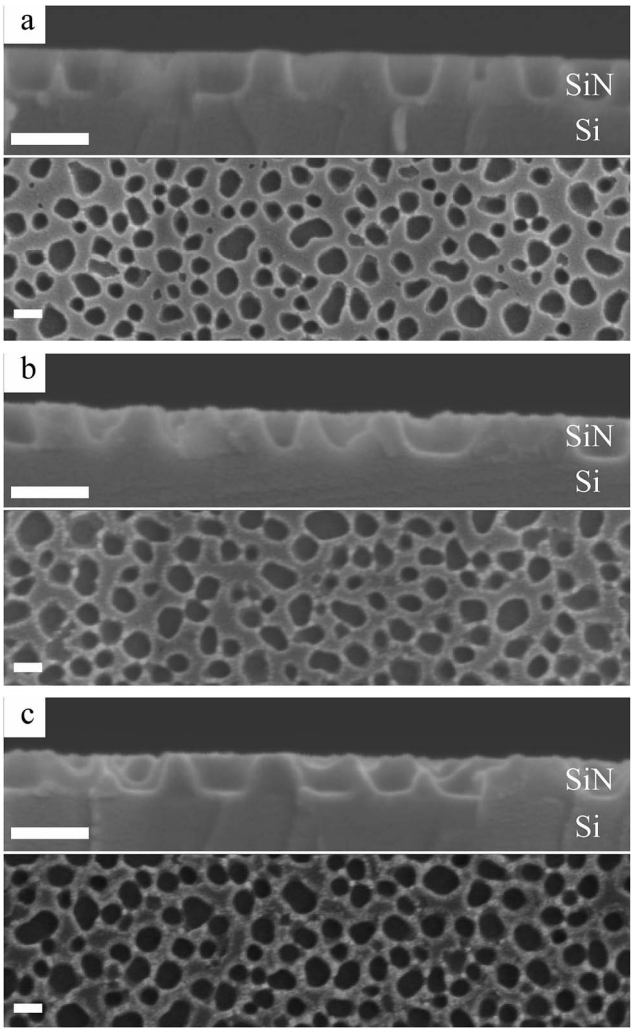

Fig. 3 SEM cross-sectional micrographs of the pores formed in a 50 nm SiN film using RIE chamber pressures of (a) 100, (b) 200 and (c) 300 mTorr with their respective top-down view micrographs. In the cross-sections, the RIE acted from top to bottom. Note that the study was performed on bulk silicon wafers and are not freestanding membranes. Scale bars equal 100 nm in both the top-down and cross-section view.

Next we examined the effects of forming the pnc-Si mask at different RTP temperatures. With conventional pnc-Si we have found that increased RTP temperatures have a greater influence on porosity than on pore size.[8] Fig. 4 shows the effect of RTP temperature on the resulting pore size of NPN. Pores are relatively constant in size (~50 nm) across three RTP temperatures (950 °C, 1000 °C, and 1050 °C), while the porosity increases dramatically from <1% at 950 °C to 22% at 1050 °C. This data indicates that the RTP temperature can significantly alter the porosity of the final NPN but has only a nominal effect on the average pore size. Based on this data, 1050 °C was selected as the RTP temperature for the remainder of our work in order to create membranes with the highest porosity.

The final process condition adjusted was the duration of the RIE process. Again, the goal was to determine the effect of the RIE duration on the pore size and porosity of the NPN. RIE etch

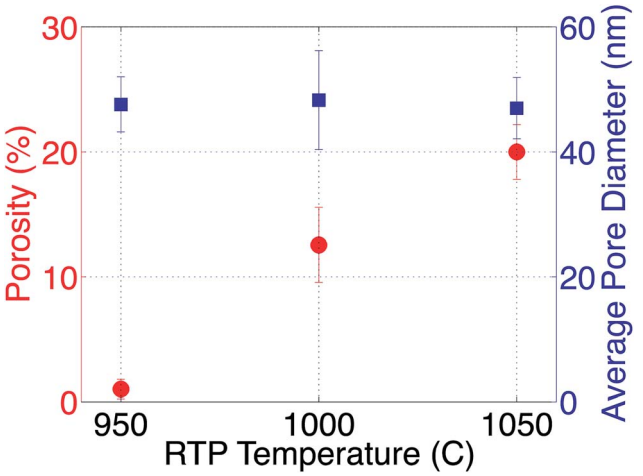

Fig. 4 A plot showing the pore size and diameter when using an RTP soak temperature of 950, 1000, and 1050 °C. Porosity increases with RTP temperature while the pore size remains consistent.

times of 0, 10, 20, 30, 40, and 50 s were used with representative TEM and SEM micrographs from the 10, 20, 30 and 40 s samples shown in Fig. 5a–d, respectively. The SEM cross-sections illustrate the depth of the RIE etch. After 10 s the RIE has extended the pore in the pnc-Si mask into the SiN film as far as 10 nm to form pits. By 20 s the pits in the SiN film have widened and gone slightly deeper, but have yet to completely traverse the SiN film. At 30 s the RIE has created through pores but has also slightly thinned the pnc-Si mask. After 40 s of RIE the pores have become larger, the pnc-Si mask has been completely etched, and the top of the SiN membrane has begun to etch, resulting in a rougher top surface for the membrane. By 50 s, the SiN was sufficiently etched that it could no longer constitute a free-standing film. The porosity and effective pore diameter as a function of RIE time are plotted in Fig. 5e.

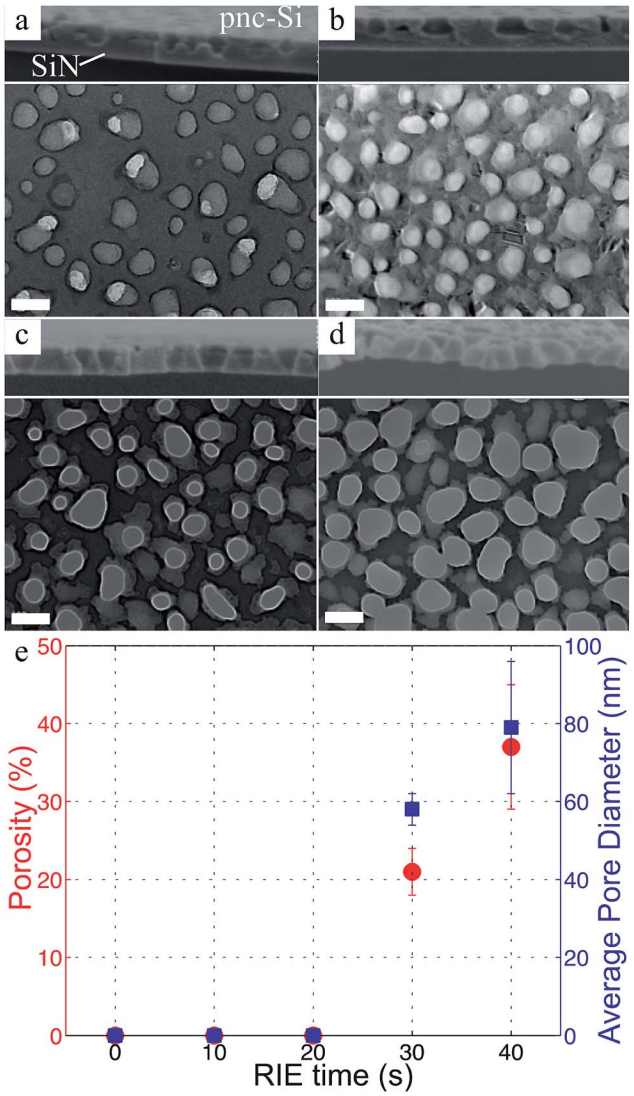

Fig. 5 TEM micrographs with insets of SEM cross-sections of samples receiving 10 s (a), 20 s (b), 30 s (c), and 40 s (d) RIE times, respectively. The cross-sections are oriented such that the top of the wafer is facing up. The white scale bars correspond to a length of 100 nm. (e) Porosity (red circles) and average pore diameter (blue squares) as a function of RIE time.

Functional testing

Before examining the utility of NPN membranes as separation tools, we first measured the more fundamental characteristics of burst pressure, gas permeance, and hydraulic permeability. Burst pressure is measured by steadily increasing the pressure of nitrogen gas applied to the "back" side of the membrane until one or more of the 5 membrane windows ruptures. Fig. 6a shows the burst pressure for samples with an RIE etch time of 0 s, 30 s, and 40 s, as well as that of traditional 40 nm pnc-Si. As expected, the burst pressure of the nonporous sample with a 0 s etch is significantly higher than the 30 s and 40 s samples that have through-pores. It is noteworthy that the 30 s etch NPN sample has a higher burst pressure than 40 nm pnc-Si, despite having a porosity more than three times higher. The reported fracture toughness of bulk Si and SiN is ~0.82–0.95 MPa$\sqrt{m}$ and 3.6–6.0 MPa$\sqrt{m}$, respectively.[23] While we do not see a 5 fold improvement in burst pressures for NPN compared to pnc-Si, we do see a clear improvement in the mechanical strength of NPN. Specifically, NPN membranes created with a 30 s etch exhibit ~2 fold higher burst pressures despite having ~3 fold greater porosity than comparably thick pnc-Si. An accurate theoretical comparison between these materials will require that we account for both porosity and nanoscale thinness. We also need to determine the maximal local stresses experienced during testing, which are certain to be higher than bust pressures.

The permeance of wafers with 0, 10, and 20 s RIE etches were either 0 mL min^{-1} cm^{-2} bar^{-1} or too low to be measured by our equipment thus confirming micrographs that indicated no evidence of through-pores (Fig. 5). The permeance (Fig. 6b) of samples with a 30 s etch was 62 000 mL min^{-1} cm^{-2} bar^{-1} and the 40 s etch sample was 235 000 mL min^{-1} cm^{-2} bar^{-1}. Theoretical predictions using an average pore diameter and pore density estimate the permeance of the 30 s and 40 s etch samples to be 56 000 mL min^{-1} cm^{-2} bar^{-1} and 184 000 mL

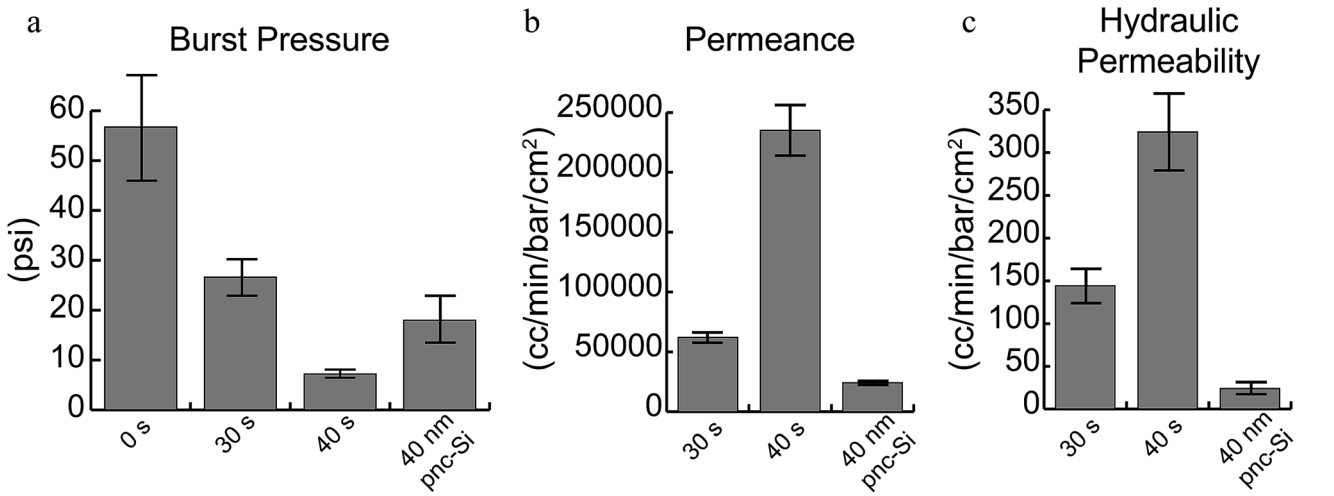

Fig. 6 (a) A plot of burst pressures for the 0 s, 30 s, and 40 s etch samples as well as traditional 40 nm pnc-Si. The burst pressure is highest for the unetched sample and then decreases with increased etch time. The 30 s etch sample has a higher burst pressure than 40 nm pnc-Si despite having three times the porosity. (b) Gas permeance and (c) hydraulic permeability, respectively, of the 30 s, 40 s, and traditional 40 nm pnc-Si. As expected, the permeance and permeability of the NPN membranes increases with increased pore size and porosity.

min^{-1} cm^{-2} bar^{-1}, respectively.[24] NPN permeance values are much higher than 40 nm pnc-Si membranes measured at ~24 000 mL min^{-1} cm^{-2} bar^{-1} (Fig. 6b).

Samples made with a 30 s RIE etch had a hydraulic permeability of 144 mL min^{-1} cm^{-2} bar^{-1} while 40 s RIE etched samples measured 324 mL min^{-1} cm^{-2} bar^{-1}. These permeability values are significantly higher than standard 40 nm pnc-Si materials (~24 mL min^{-1} cm^{-2} bar^{-1}) because of the higher porosity and pore sizes of NPN. The measured hydraulic permeability values are plotted in Fig. 6c. The values are also in reasonable agreement with theoretical predictions which estimates the hydraulic permeability for the 30 and 40 s samples to be 168 mL min^{-1} cm^{-2} bar^{-1} and 490 mL min^{-1} cm^{-2} bar^{-1}, respectively.[9] Note that both the hydraulic permeability (0.3 mL min^{-1} cm^{-2} bar^{-1}) and permeance (109 mL min^{-1} cm^{-2} bar^{-1}) values of track-etched membranes with comparable pore sizes are orders-of-magnitude lower than NPN (http://www.sterlitech.com).

Next we investigate the ability of NPN membranes to filter Au NPs of various sizes (Fig. 7). Filtrations were performed with a gold nanoparticle size ladder (10 nm; 20 nm; 40 nm; 50 nm; 60 nm; 80 nm; 100 nm diameter) to determine a cut-off and resolution for the two porous samples (30 s and 40 s RIE). The NPN membrane made with a 30 s etch displays a cutoff between 40 and 50 nm, and the sample receiving a 40 s RIE etch has a larger cutoff between 60 and 80 nm. Both cut-offs appear 'sharp,' displaying at least 80% reduction in transmission between two consecutive NP sizes in the ladder. Using the value of these consecutive particle sizes it is possible to say the 'resolution' of the 30 s membrane is at least 10 nm and the resolution of the 40 s RIE membrane is at least 20 nm. Using a higher resolution gold nanoparticle ladder, Gaborski *et al.*, found that pnc-Si membranes with pore size cut-offs smaller than 30 nm exhibited a resolution of ~5 nm in separation experiments. A larger cut-off is expected for NPN because the pores are significantly larger than for pnc-Si. Because our evaluation of the resolution

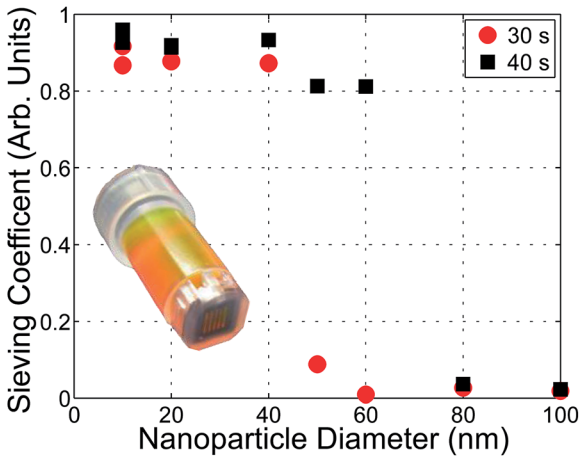

Fig. 7 A plot of sieving coefficient *versus* Au nanoparticle diameter. The cutoff of the 30 s RIE sample is between 40 and 60 nm while the cutoff for the 40 s RIE sample is somewhere between 60 and 80 nm. The inset is a photo of the spin cup assembly used in separations.

of NPN membranes is limited by the 10 or 20 nm step-size of the gold ladder used here, further experiments are needed to determine if the resolution of NPN is actually better than 10 nm.

While the membrane cut-offs correlate with the relative pore sizes of the two NPN membranes, neither the average pore sizes (58 nm for 30 s RIE; 79 nm for 40 s RIE), nor the maximum pore sizes (100 nm for 30 s RIE; 120 nm for 40 s RIE) are predictive of the actual cut-off. This is expected for gold filtration in deionized water as the electrostatic and electrokinetic interactions between charged nanoparticles and membranes make the effective pore sizes smaller than their physical dimensions.[9] The method of the pore diameter calculation likely also plays a role in explaining the disparity between the effective and physical pore dimensions. Our custom image processing program determines the area of the pore and calculates the diameter

assuming the pore is perfectly circular, which holds reasonably well for pnc-Si.[7,8] As seen in the TEM micrograph in Fig. 5 however, many pores in NPN are not perfectly circular due to pore merging during the etch process. In the case of oblong or irregularly shaped pores, the cut-off is actually determined by the minimum span of the pore.

Cell growth analysis

In addition to uses as a filtration material, pnc-Si has found use as a highly permeable cell culture and co-culture substrate.[10] To determine if NPN nanomembranes can also be used for cell culture applications, we examined the adhesion and growth of human umbilical vein vascular endothelial cells (HUVEC) on the samples created by different RIE times (Fig. 8). The unetched (0 s in Fig. 8a) surfaces show excellent early cell attachment and spreading, and proliferation and cell morphology after 2 days that are typical of cultured endothelial cells. These results are not surprising because without membrane exposure to RIE, the cells adhere and grow on the pnc-Si template. For samples in which the pnc-Si layer was partially etched with a 20 s or 30 s RIE (Fig. 8b and c), the initial cell adhesion was delayed compared to the unetched samples. Adhesion was also delayed on membranes where XeF_2 was used to completely remove the pnc-Si template layer leaving a smooth SiN surface behind (8d; see methods). Also it has been shown by others that untreated silicon nitride is an unfavorable substrate for cell adhesion and growth, and that surface functionalization is essential for most biological applications.[25] It appears that the SiN surface is eventually modified by the passive adsorption of proteins from culture serum however, because cells do eventually attach and grow on SiN membranes with no obvious difference in the morphology compared to the unetched material. An exception to this rule is the over-etched (40 s RIE) material. Because the 40 s etch duration removes the pnc-Si capping layer and also partially etches the silicon nitride, it leaves a rough porous silicon nitride surface for the cells to grow on. This surface appeared to be the least favorable in terms of both cell attachment and ultimate cell morphology (Fig. 8e). The results suggest that functionalization of NPN membranes with molecules that promote cell adhesion would improve their utility as tools for cell culture.

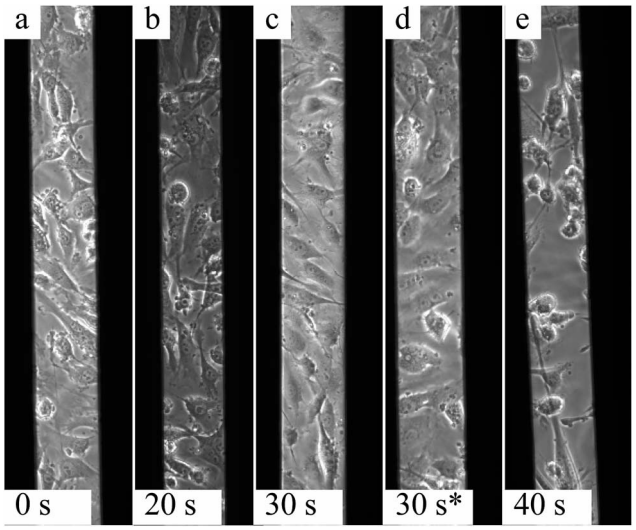

Fig. 8 Phase contrast images of endothelial cells grown on samples after three to five days with varying morphology due to different RIE times. (a) On the 0 s RIE sample the HUVECs were able to adhere, grow and proliferate on the pnc-Si surface as previously shown. Cells also adhere and grow on samples produced with 20 s (b) or 30 s (c) RIE etch, although the initial cell adhesion appears delayed compared to pnc-Si. Complete removal of the pnc-Si cap using a XeF_2 etch on a 30 s RIE sample (d) gave similar results to an untreated 30 s etch. Over etching at 40 s RIE shows that exposure of the rough silicon nitride surface inhibits cell attachment and growth (e).

Conclusions

We have developed a highly scalable method for fabricating ultrathin nanoporous nitride (NPN) membranes using porous nanocrystalline silicon (pnc-Si) as a self-assembling template for pore transfer by RIE. The membranes display the high flow rates and sharp cut-offs associated with ultrathin silicon membranes,[7,9] with the added strength and chemical robustness of SiN. NPN membranes have higher burst pressures and 5× greater permeability than pnc-Si while maintaining a similar separation resolution (<10 nm). Pore sizes and porosity can be controlled by adjusting the pressure and etch time of the RIE transfer process or using different annealing temperatures in the formation of the pnc-Si template. In addition to filtration, ultrathin silicon membranes have found applications in cell culture.[10] Here we show that cells can adhere and grow on NPN as well, although extensive etching that results in a rough nitride surface appears to hinder adhesion. Additionally, the membranes can have the masking pnc-Si removed chemically to leave a smooth SiN surface.

Experimental

Fabrication

Double-side polished silicon wafers (⟨100⟩ oriented, 100 mm diameter), were first coated on both sides with 50 nm SiN using LPCVD with a target tensile stress of 250 MPa. Using a standard RF sputtering process in an AJA ATC 2000 V Sputtering system (North Scituate, MA), the frontside SiN was then covered with a 40 nm-thick amorphous silicon film followed by 20 nm-thick SiO_2 film, as shown in Fig. 8a. Unless otherwise noted, the wafers were then annealed using a rapid thermal process (RTP; Surface Science Integration Solaris 150, El Mirage, Az) with a target soak temperature of 1050 °C for 60 s in order to transform the amorphous silicon into pnc-Si. The RTP chamber was filled with nitrogen and was heated at a ramp rate of 100 °C s^{-1}. Fig. 2 illustrates how the backside SiN was patterned using standard photolithography and an RIE process flowing 50 sccm SF_6 and 100 sccm Ar to expose the bulk silicon. The frontside SiO_2 layer acts to protect the pnc-Si and SiN films during the backside processing. Following the backside patterning, the frontside 20 nm SiO_2 layer was removed using a 45 s 10 : 1 buffered oxide etch (BOE) immersion to reveal the pnc-Si and SiN films

underneath. The resulting structure was a 40 nm pnc-Si hard mask above a solid 50 nm SiN film on the bulk silicon surface.

The nanopores present in the pnc-Si film were then transferred into the SiN layer below using an anisotropic RIE, as seen in Fig. 2. For an effective pattern transfer, an RIE recipe which is highly selective to SiN over Si was required. CHF_3, flown at a rate of 50 sccm, was chosen as the main etchant. The hydrogen present in the CHF_3 gas is known to increase the etch resistance of the silicon, while the carbon and fluorine mixture succeeded in etching the nitride at nearly twice the rate.[26] The hydrogen present in the CHF_3 also protects the bulk silicon from being etched, providing an excellent etch stop. 5 sccm oxygen and 100 sccm argon were also included in the gas mixture to increase the anisotropy of the etch.

A 100 nm-thick SiO_2 layer was deposited atop the NPN by PECVD using a TEOS prescursor gas. The wafer is then placed in a single-sided etch cell where ethylenediamine pyrocatechol (EDP) is exposed to the patterned back side. This SiO_2 film acted as a temporary protective layer to keep the from reaching the front surface during the final minutes of the bulk Si wafer etch. Once the windows are completely cleared of Si, the wafer is removed from the EDP etch cell and thoroughly rinsed with water. Finally, a 10 : 1 BOE immersion removes the remaining SiO_2 and the freestanding NPN films are revealed.

Permeance tests

Permeance was measured by flowing nitrogen gas at a constant pressure through a sample. The back side of the chip was pressurized and the front side of the chip is exposed to atmosphere. The nitrogen pressure was monitored using a manometer (VWR model 33500-084). Chips from each wafer were measured at pressures ranging from 0.5 to 5 psi. The flow rate was measured with a rotameter (Omega FL-3803ST). The rotameter was fitted with either a #042-15-N tube for samples with flow rates from 5–60 mL min^{-1} or a #082-03-N tube for samples with flow rates from 100–1700 mL min^{-1} (Omega; Stamford, CT).

Hydraulic permeability

Hydraulic permeability was tested by measuring the flow rate of Invitrogen Ultrapure water through a sample. A constant pressure from nitrogen gas was applied to a column of water containing a sample. All of the tubing containing water was kept horizontal to avoid additional pressure caused by gravity. The tubing on the exit side of the sample was connected to a VWR $1 \times 1/100$ mL serological pipet. The flow rate was determined by measuring the volume of water that moved through the pipette in a given time. A pressure of 10 psi was used for the 30 s etch samples and 3 psi was used for the 40 s etch samples in order to maximize flow while minimizing the risk of breaking a sample.

Separations

Separations were accomplished by mounting chips into a custom plastic housing as pictured in the inset of Fig. 7. In this separation study, Invitrogen Ultrapure water was used to dilute Au NPs of 10, 20, 40, 50, 60, 80 and 100 nm diameters to concentrations of 1.4×10^{12}, 1.8×10^{11}, 2.2×10^{10}, 1.1×10^{10}, 6.5×10^{9}, 2.8×10^{9} and 1.4×10^{9} particles/mL, respectively (BBI Solutions; Cardiff, UK). Separations were initially attempted using a centrifuge, but it was found that NPs with a diameter of 50 nm or greater would pellet out of solution and accumulate along the side of the plastic housing. In order to avoid this pelleting, flow through the membrane was induced by applying constant pressure to the top reservoir with nitrogen gas. The top reservoir was filled with 300 μL of Au NP solution. The bottom reservoir was filled with 12 μL of water in order to wet the pores and facilitate flow through the pores. Initially, pure water was passed through the filters to ensure complete wetting of the membrane and viability of the assembly. Following the water, the solution of Au NPs was introduced. The filtrate was collected and weighed in order to mathematically compensate for the additional 12 μL introduced into the solution. The relative concentration of Au solutions was analyzed by optical absorbance measurements in the visible spectrum in a Tecan infinite m200 (Mannedorf, Switzerland). The sieving coefficient, S, was calculated by dividing the intensity at the highest value of the absorbance peak of the filtrate by that of the initial solution.

Cell culture

Immortalized human umbilical vein endothelial cells (HUVECs) were obtained from Vaccinex Inc, Rochester, NY. Cells were grown in DMEM media (Mediatech Inc. VA), with 10% fetal bovine serum (Gibco, Grand Island, NY), and 1% penicillin and streptomycin (Gibco, Grand Island, NY). Cells were grown until confluence at 37 °C in 80% RH and 5% CO_2 environment. For testing the cell growth on different Si and SiN surfaces, cells were trypsinized and seeded on to the test surfaces. MCDB-131 Complete media (Vec Technologies, Rensselaer, NY) was used for facilitating growth on the different test surfaces. This media consists of complete media supplemented with serum, antibiotics as well as endothelial growth factor to facilitate better cell adhesion and proliferation.

To remove the remaining 10 nm of pnc-Si on the 30 s etch sample, a Xactix E-1 XeF_2 etcher was used. The samples were subjected to a 2.2 Torr N_2 pulse followed by a 2.2 Torr XeF_2 pulse for a single 60 second etch cycle. All the surfaces were subjected to post-production thermal processing step in RTP. The samples were treated in a SiC coated susceptor. The temperature was increased at the rate of 10 °C s^{-1} up to 800 °C and then kept constant for 5 minutes. All the samples were autoclaved for sterility and were used in a 24-well tissue culture plate. Imaging was performed following 2–4 days after cell seeding using Nikon TS-100F inverted microscope (Tokyo, Japan).

Acknowledgements

The authors would like to thank Brian McIntyre and URnano for help with material deposition and electron microscopy, as well as the staff at RIT's Semiconductor and Microsystems Fabrication Laboratory. This work was funded by the National Science Foundation, GOALI #1159579. A corporate start-up, SiMPore Inc., participated in this work. SiMPore plans to make the NPN membrane material commercially available. J.M. and T.G are

founders of SiMPore. C.C. and J.D. were employed by SiMPore during this project and helped design and produce custom membrane chips for the study. The authors thank the entire Nanomembrane Research Group (nanomembranes.org) for helpful discussions throughout the development of NPN.

Notes and references

1 J. Y. Han, J. P. Fu and R. B. Schoch, *Lab Chip*, 2008, **8**, 23–33.
2 P. Stroeve and N. Ileri, *Trends Biotechnol.*, 2011, **29**, 259–266.
3 A. van den Berg and M. Wessling, *Nature*, 2007, **445**, 726.
4 A. Mehta and A. L. Zydney, *J. Membr. Sci.*, 2005, **249**, 245–249.
5 D. M. Malone and J. L. Anderson, *Chem. Eng. Sci.*, 1978, **33**, 1429–1440.
6 B. H. Winkler and R. E. Baltus, *J. Membr. Sci.*, 2003, **226**, 75–84.
7 C. C. Striemer, T. R. Gaborski, J. L. McGrath and P. M. Fauchet, *Nature*, 2007, **445**, 749–753.
8 D. Z. Fang, C. C. Striemer, T. R. Gaborski, J. L. McGrath and P. M. Fauchet, *J. Phys.: Condens. Matter*, 2010, **22**, 454134.
9 T. R. Gaborski, J. L. Snyder, C. C. Striemer, D. Z. Fang, M. Hoffman, P. M. Fauchet and J. L. McGrath, *ACS Nano*, 2010, **4**, 6973–6981.
10 A. A. Agrawal, B. J. Nehilla, K. V. Reisig, T. R. Gaborski, D. Z. Fang, C. C. Striemer, P. M. Fauchet and J. L. McGrath, *Biomaterials*, 2010, **31**, 5408–5417.
11 J. L. Snyder, J. Getpreecharsawas, D. Z. Fang, T. R. Gaborski, C. C. Striemer, P. M. Fauchet, D. A. Borkholder and J. L. McGrath, *Proc. Natl. Acad. Sci. U. S. A.*, 2013, **110**, 18425–18430.
12 M. N. Kavalenka, C. C. Striemer, J. P. S. DesOrmeaux, J. L. McGrath and P. M. Fauchet, *Sens. Actuators, B*, 2012, **162**, 22–26.
13 H. Yamazaki, S. Kimura, M. Tsukahara and K. Esashika, *Appl. Phys. A: Mater. Sci. Process.*, 2014, **115**, 53–56.
14 D. G. Johnson, T. S. Khire and Y. L. Lyubarskaya, *Adv Chron Kidney Dis*, 2013, **20**, 508–515.
15 C. vanRijn, M. vanderWekken, W. Nijdam and M. Elwenspoek, *J. Microelectromech. Syst.*, 1997, **6**, 48–54.
16 H. D. Tong, H. V. Jansen, V. J. Gadgil, C. G. Bostan, E. Berenschot, C. J. M. van Rijn and M. Elwenspoek, *Nano Lett.*, 2004, **4**, 283–287.
17 I. Vlassiouk, P. Y. Apel, S. N. Dmitriev, K. Healy and Z. S. Siwy, *Proc. Natl. Acad. Sci. U. S. A.*, 2009, **106**, 21039–21044.
18 W. H. Liu, M. Ferguson, M. Yavuz and B. Cui, *J. Vac. Sci. Technol., B: Nanotechnol. Microelectron.: Mater., Process., Meas., Phenom.*, 2012, **30**, 06F201.
19 F. Montagne, N. Blondiaux, A. Bojko and R. Pugin, *Nanoscale*, 2012, **4**, 5880–5886.
20 M. Cheryan, *Ultrafiltration handbook*, Technomic Pub. Co., Lancaster, Pa., 1986.
21 B. P. Nabar, Z. Celik-Butler, B. H. Dennis and R. E. Billo, *J. Micromech. Microeng.*, 2012, **22**, 045012.
22 C. Qi, C. C. Striemer, T. R. Gaborski, J. L. McGrath and P. M. Fauchet, *Small*, 2014, **10**, 2946–2953.
23 W. D. Callister, *Materials science andengineering: an introduction*, John Wiley & Sons, New York, 7th edn, 2007.
24 M. N. Kavalenka, C. C. Striemer, D. Z. Fang, T. R. Gaborski, J. L. McGrath and P. M. Fauchet, *Nanotechnology*, 2012, **23**, 22–26.
25 J. J. M. Benavente, H. Mogami, T. Sakurai and K. Sawada, *PLoS One*, 2014, **9**, e90189.
26 B. D. Pant and U. S. Tandon, *Plasma Chem. Plasma Process.*, 1999, **19**, 545–563.